Applicability of Accurate Ground Motion Estimation Using Initial P Wave for Earthquake Early Warning

Zijun Wang[1,2] and Boming Zhao[1,2]*

[1]Key Laboratory of Urban Underground Engineering of Ministry of Education, Beijing Jiaotong University, Beijing, China, [2]School of Civil Engineering, Beijing Jiaotong University, Beijing, China

The earthquake early warning (EEW) system is capable of mitigating seismic hazards and reducing deaths, injuries, and economic losses. Although EEW approaches have already been developed worldwide, improving the accuracy and applicability is still controversial. Aiming at the ground motion estimation using the initial P wave, we investigated eight representative characteristic parameters, i.e., the peak measurements and integral quantities, using the database of the 2008 Wenchuan earthquake, where the aftershocks with the criteria that $4.0 \leq Ms \leq 6.5$ and epicentral distance less than 150 km are analyzed. We established the relationships between the eight characteristic parameters and four ground motion parameters, respectively, based on which the estimation accuracy and reliability and the extent to which the increasingly expanding time windows could affect the estimates are analyzed accordingly. We found that the integral quantities could also be a robust estimator for peak ground acceleration (PGA), peak ground velocity (PGV), and spectral intensity (SI), while the peak measurement is more useful in estimating peak ground displacement (PGD). In addition, for estimating the ground motion of events with magnitudes less than 6.5, a 2-s window could effectively improve the estimation accuracy by approximately 11.5–18.5% compared with using a 1-s window, as the window increases to 3 s, the accuracy would further improve while the growth rate will be reduced to around 3.0–8.0%.

Keywords: earthquake early warning, ground motion estimation, Wenchuan earthquake, initial P wave, characteristic parameters

INTRODUCTION

The earthquake early warning (EEW) system is capable of mitigating seismic hazards and reducing deaths, injuries, and economic losses (Allen and Melgar, 2019; Zollo et al., 2016; Hoshiba, 2014). By regional and on-site algorithms, alerts could be sent ahead of the earthquake events induced ground shaking at target locations so that appropriate measures can be taken immediately against seismic hazards (Cremen and Galasso, 2020; Satriano et al., 2011), e.g., slowing the high-speed trains to reduce accidents and shutting down gas valves to prevent fires in a short term. The EEW systems are generally regarded as positive measures by relevant stakeholders that many earthquake-prone countries and regions are operating or testing their own systems.

The regional approach leverages the information from the seismic network deployed next to the epicenter to evaluate the relevant source parameters (event location and magnitude) and predict the regional seismic intensities using the traditional ground motion prediction equation (GMPE)

**TABLE 1** | Seismic events studied in this paper.

No.	Origin time (UT)		Latitude	Longitude	Focal depth (km)	Ms	Number of records
1	2008.08.05	17:49:16	32.72	105.61	13	6.5	5
2	2008.05.25	16:21:47	32.55	105.48	14	6.4	6
3	2008.05.12	14:43:15	31.27	103.82	14	6.3	7
4	2008.05.12	19:11:01	31.26	103.67	14	6.3	15
5	2008.08.01	16:32:42	32.02	104.85	14	6.2	4
6	2008.05.13	15:07:08	30.95	103.42	14	6.1	12
7	2008.05.18	1:08:24	32.2	105.08	13	6.1	8
8	2008.07.24	15:09:28	32.76	105.61	10	6	3
9	2008.05.12	14:54:17	31.26	103.59	13	5.8	4
10	2008.05.12	15:34:42	31.29	103.77	13	5.8	7
11	2008.05.27	16:37:51	32.78	105.7	15	5.7	3
12	2008.07.24	3:54:43	32.72	105.63	10	5.7	2
13	2008.05.12	15:01:34	31.45	104.49	13	5.5	6
14	2008.05.12	16:10:57	31.14	103.6	10	5.5	3
15	2008.05.12	16:21:40	31.53	104.28	11	5.5	11
16	2008.05.13	7:46:18	31.34	103.58	13	5.4	13
17	2008.05.12	17:42:24	31.48	104.13	14	5.3	10
18	2008.05.27	16:03:22	32.76	105.65	15	5.3	5
19	2008.05.12	16:35:05	31.29	103.65	14	5.2	3
20	2008.05.12	17:06:59	31.16	103.69	10	5.2	4
21	2008.05.12	17:31:15	31.16	103.56	10	5.2	6
22	2008.05.12	16:26:12	31.4	104.12	12	5.1	7
23	2008.05.12	16:47:23	32.16	105.12	9	5.1	3
24	2008.05.12	22:46:06	32.72	105.64	10	5.1	8
25	2008.05.12	17:23:35	32.19	104.92	20	5	3
26	2008.05.12	18:23:39	30.97	103.48	9	5	8
27	2008.05.12	19:33:20	32.55	105.35	16	5	5
28	2008.05.13	1:29:06	31.21	103.68	24	4.9	12
29	2008.05.12	16:50:39	32.24	105.19	21	4.8	3
30	2008.05.13	2:26:17	31.47	104.1	11	4.8	4
31	2008.05.12	19:52:25	32.71	105.36	20	4.7	3
32	2008.05.12	20:29:58	31.4	104.07	11	4.6	4
33	2008.05.13	0:28:53	31.26	103.76	16	4.5	4
34	2008.05.13	13:36:29	32.47	105.23	11	4.4	3
35	2008.05.12	20:15:40	31.87	104.57	9	4.3	10
36	2008.05.12	20:11:59	31.32	104.24	15	4.2	7
37	2008.05.13	7:43:51	31.37	104.34	14	4	3

(Satriano et al., 2011). While on the other hand, the on-site system often consists of a limited set of seismic stations located at particular target sites of interest, which typically provide rapid ground motion estimates, using only information on the characteristics of P waves recorded at one seismic station, where an early warning is often most needed (Kanamori, 2005). A number of algorithms account for the uncertainties of ground motion estimation by considering a confidence interval on the estimate with width equivalent to two standard deviations of the empirical relationship used to derive ground shaking (Wu and Kanamori, 2005; Wu and Kanamori, 2008; Zollo et al., 2010; Zollo et al., 2016).

Western China is an earthquake-prone area with high intensity and frequency, which poses a great threat to the city and transportation system (Xu et al., 2009). For instance, most of the high-speed railways in China have no choice but to be constructed in the areas of moderate to high level of seismic fortification intensity, being prone to derail or overturn in case of dynamic actions and causing catastrophic hazards, even in small seismic events. Effective detection of these events is a necessary condition for disaster prevention and mitigation. However, since China is of a vast territory, it is not possible to set up dense strong ground motion station networks on a large scale at present, and for infrastructures such as high-speed railway which is linearly distributed, it is required to investigate the approach that can be used for single station, which is also expected to improve the reliability of an on-site system, where no information or constraint on the earthquake source is available in real-time.

In this paper, aiming at the ground motion estimation using the initial P wave and among the possible parameters measurable in real-time, i.e., the peak measurements and the integral quantities, we investigated eight representative parameters using the database of the 2008 Wenchuan earthquake (China Strong Motion Networks Centre, 2020). The estimation accuracy and reliability in the established relationships toward four different ground motion parameters are analyzed, respectively. To further investigate that to what an extent the initial signal window length could affect the estimates, we compared the variation tendency of standard deviation and determination coefficient between the leading parameters and the corresponding ground motion parameters of different time window. We found that the integral quantities could also be a robust estimator for PGA, PGV
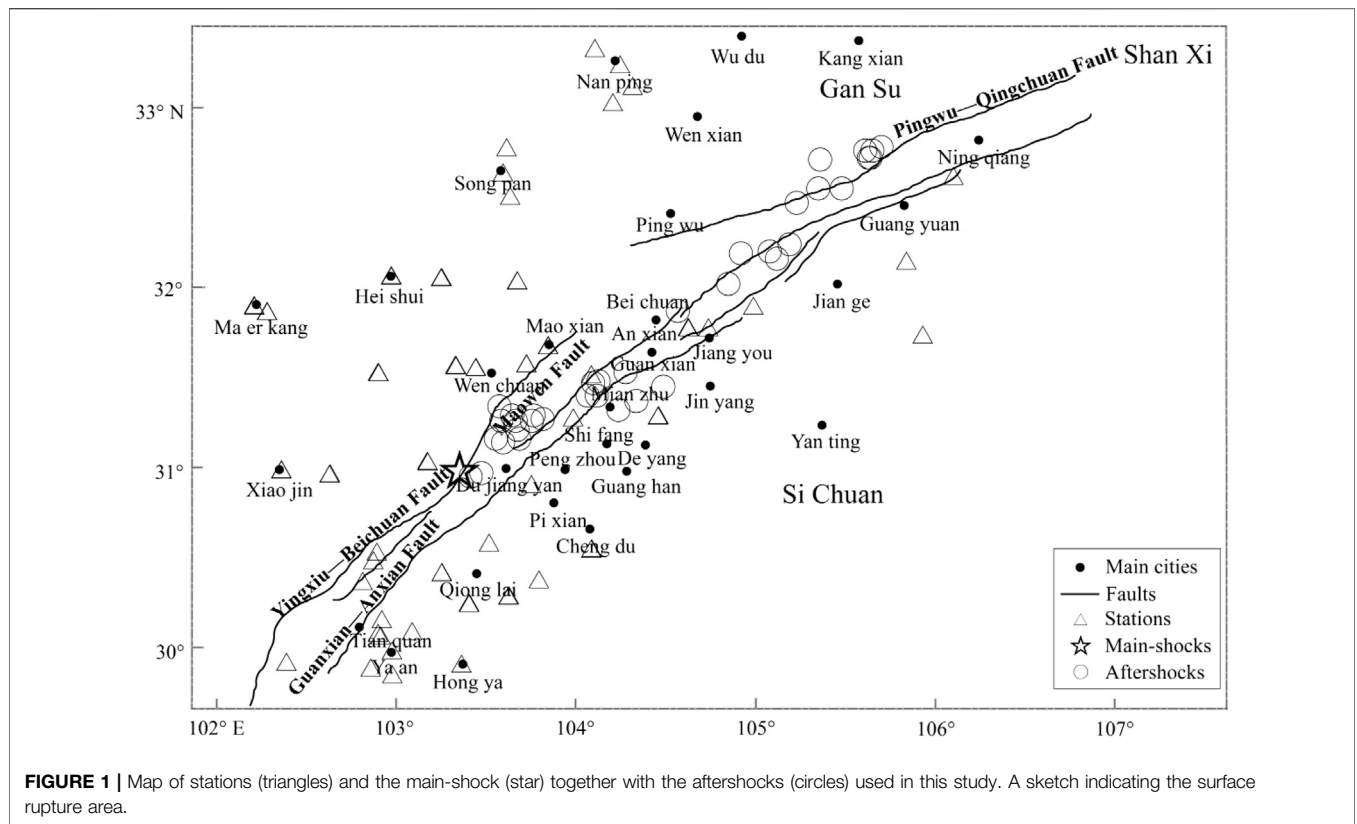
FIGURE 1 | Map of stations (triangles) and the main-shock (star) together with the aftershocks (circles) used in this study. A sketch indicating the surface rupture area.

TABLE 2 | Regression coefficients of the characteristic parameters and PGA.

(s)	PGA	P_a	P_v	P_d	IA2	IV2	ID2	CAV	si
1	A	0.730	0.771	0.557	0.372	0.384	0.238	0.748	0.743
	B	0.561	1.844	2.187	0.907	2.162	2.126	0.982	1.572
	stv	0.244	0.245	0.355	0.245	0.260	0.382	0.245	0.274
	R^2	0.723	0.719	0.410	0.719	0.683	0.317	0.720	0.684
2	A	0.786	0.791	0.564	0.413	0.397	0.250	0.831	0.760
	B	0.463	1.811	2.154	0.745	2.073	2.094	0.712	1.467
	stv	0.205	0.231	0.347	0.200	0.244	0.371	0.203	0.248
	R^2	0.803	0.751	0.436	0.813	0.722	0.357	0.808	0.703
3	A	0.814	0.786	0.535	0.429	0.400	0.246	0.867	0.776
	B	0.417	1.774	2.056	0.653	2.008	2.009	0.542	1.410
	stv	0.195	0.227	0.354	0.184	0.238	0.369	0.186	0.245
	R^2	0.823	0.760	0.414	0.843	0.735	0.362	0.841	0.731

Note: R^2 is the coefficient of determination.

and SI, while the peak measurement is more useful in estimating PGD. In addition, we show that for estimating the ground motion of events with magnitudes less than 6.5, a 1 s of P wave is not enough, while a 2-s window could effectively improve the estimation accuracy, as the window increases to 3 s, the accuracy would further improve while the growth rate is not that much.

DATA AND PRE-PROCESSING

The 2008 Ms 8.0 Wenchuan earthquake provided an opportunity to collect sound qualified data in a large scale that China Strong Motion Net Centre (CSMNC) recorded 383 aftershocks until September 30, 2008 (China Strong Motion Networks Centre, 2020). More than 600 cases with magnitudes above Ms 4.0 were acquired, among them 56 aftershocks were larger than Ms 5.0 and 8 aftershocks, larger than Ms 6.0. These events were over a rupture length of about 300 km with focal depths ranging from 2 to 20 km. Since the near-fault records of the destructive earthquakes are most important for the EEW system purposes (Nakamura et al., 2011; Satriano et al., 2011), we then selected 37 aftershocks with the criteria that Ms greater than 4.0 and epicentral distance less than 150 km. However, some traces were not recorded from the very beginning that the first P wave arrivals were lost, which were not satisfied with the aim of our study and these cases were discarded.

These records were obtained by the strong motion seismographs with a dynamic range of ±2 g mainly installed at free-field sites and the sampling rate was 200 Hz. We used the proposed three-step detection method to pick the P wave in real-time (Wang and Zhao, 2017) and double checked the arrival time by manual inspection for each waveform. In addition, each record has been checked that the signal noise ratio (SNR) above three is finally adopted (Küperkoch et al., 2010). With the detected P wave, the corresponding early-measured attributes could be calculated based on their formulas or physical meanings. The seismic events studied in this paper are listed in **Table 1** while the distributions of these events along the ruptures with the stations are shown in **Figure 1**.

TABLE 3 | Regression coefficients of the characteristic parameters and PGV.

(s)	PGV	P_a	P_v	P_d	IA2	IV2	ID2	CAV	si
1	A	0.613	0.770	0.721	0.310	0.398	0.325	0.626	0.740
	B	−0.947	0.289	1.029	−0.656	−0.655	1.043	−0.594	0.009
	stv	0.349	0.278	0.289	0.352	0.272	0.322	0.350	0.320
	R^2	0.472	0.665	0.639	0.464	0.680	0.552	0.468	0.556
2	A	0.690	0.818	0.727	0.362	0.426	0.336	0.730	0.814
	B	−1.044	0.289	0.977	−0.796	0.609	0.968	−0.825	−0.051
	stv	0.313	0.244	0.275	0.312	0.230	0.305	0.312	0.272
	R^2	0.574	0.743	0.672	0.579	0.771	0.598	0.577	0.682
3	A	0.728	0.822	0.736	0.385	0.434	0.331	0.779	0.864
	B	−1.091	0.263	0.887	−0.881	0.552	0.859	−0.980	−0.078
	stv	0.300	0.229	0.262	0.292	0.213	0.300	0.292	0.248
	R^2	0.609	0.772	0.702	0.631	0.803	0.610	0.630	0.742

TABLE 4 | Regression coefficients of the characteristic parameters and PGD.

(s)	PGD	P_a	P_v	P_d	IA2	IV2	ID2	CAV	si
1	A	0.439	0.712	0.928	0.211	0.376	0.445	0.431	0.542
	B	−1.749	−0.658	0.653	−1.543	−0.291	0.812	−1.499	−1.049
	stv	0.588	0.520	0.397	0.593	0.511	0.405	0.592	0.575
	R^2	0.139	0.326	0.607	0.123	0.349	0.592	0.127	0.176
2	A	0.578	0.831	0.976	0.300	0.446	0.472	0.604	0.713
	B	−1.859	−0.567	0.680	−1.652	−0.202	0.772	−1.676	−0.997
	stv	0.556	0.474	0.350	0.556	0.454	0.360	0.557	0.526
	R^2	0.231	0.441	0.696	0.229	0.486	0.678	0.227	0.311
3	A	0.640	0.842	0.980	0.344	0.465	0.473	0.695	0.797
	B	−1.916	−0.586	0.541	−1.733	−0.229	0.655	−1.822	−1.001
	stv	−0.541	0.464	0.338	0.535	0.434	0.339	0.535	0.494
	R^2	0.271	0.465	0.715	0.288	0.530	0.715	0.288	0.392

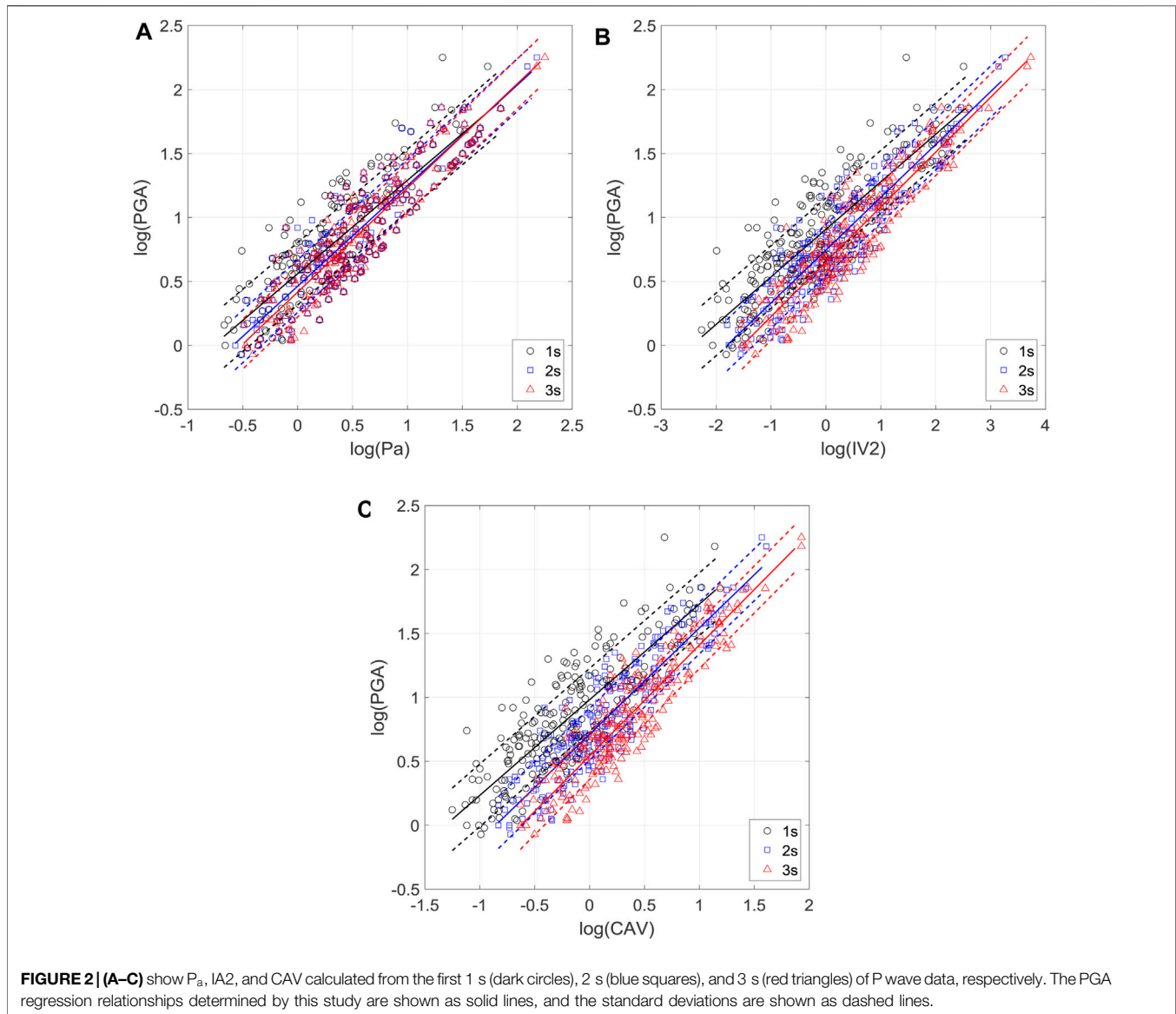**TABLE 5 |** Regression coefficients of the characteristic parameters and SI.

(s)	SI	P_a	P_v	P_d	IA2	IV2	ID2	CAV	si
1	A	0.582	0.755	0.736	0.293	0.393	0.334	0.593	0.676
	B	−0.400	0.804	1.600	−0.124	1.173	1.623	−0.065	0.487
	stv	0.369	0.295	0.284	0.372	0.285	0.317	0.371	0.352
	R^2	0.418	0.629	0.655	0.408	0.653	0.571	0.413	0.470
2	A	0.662	0.806	0.746	0.347	0.423	0.346	0.700	0.754
	B	−0.495	0.810	1.555	−0.258	1.133	1.551	−0.286	0.443
	stv	0.335	0.260	0.267	0.334	0.243	0.297	0.335	0.298
	R^2	0.520	0.711	0.696	0.524	0.747	0.623	0.522	0.606
3	A	0.701	0.812	0.755	0.372	0.431	0.339	0.753	0.842
	B	−0.542	0.786	1.462	−0.340	1.080	1.430	−0.436	0.445
	stv	0.322	0.247	0.253	0.314	0.226	0.295	0.315	0.257
	R^2	0.557	0.741	0.727	0.579	0.782	0.629	0.578	0.712

After the baseline error correction for the acceleration records, the signals were integrated to velocity records, and velocity records to displacement records, since they were required in the characteristic parameter calculations. Then, we applied a causal two-pole Butterworth filter with a cut-off frequency of 0.075 Hz on the vertical component to remove the undesired long-period trends after numerical integration (Boore et al., 2002). Zollo et al. (2010) have shown that this cut-off frequency preserves a scaling of the EEW parameters with magnitude in a broad range.

EEW Parameters Versus Ground Motion Parameters

The strengths of critical ground motions can be defined by the shock wave, where its effects are practically represented by the peak

FIGURE 2 | **(A–C)** show P$_a$, IA2, and CAV calculated from the first 1 s (dark circles), 2 s (blue squares), and 3 s (red triangles) of P wave data, respectively. The PGA regression relationships determined by this study are shown as solid lines, and the standard deviations are shown as dashed lines.

ground acceleration (PGA), peak ground velocity (PGV), and peak ground displacement (PGD). In addition, the spectral intensity (SI) is defined as follows by Housner who regarded it as a seismic index reflecting the earthquake destructive power (Housner, 1952):

$$SI_\zeta = \int_{0.1}^{2.5} S_v(T, \zeta) dT, \tag{1}$$

where S$_v$ is the relative velocity response spectrum of a single-degree-of-freedom system, T is the period, and ζ is the damping ratio which was set as 0.05 herein.

Therefore, for the EEW purposes, we used the PGA, PGV, PGD, and SI as parameters to assess the strengths of the ground motions during earthquake damage.

Normally a certain time window following the initial P wave arrival time t$_i$ is used to determine the early-measured parameters, and among the possible parameters measurable in

real-time, they could be categorized according to the signal type on which they are measured or their physical interpretation. The peak measurements, for example, the use of the peak displacement (P$_d$), peak velocity (P$_v$), or peak acceleration (P$_a$), of the first few seconds of the P wave have been shown to scale with ground motion (Colombelli et al., 2015; Bose et al., 2009). On the other hand, the integral quantities, for instance, the cumulative absolute velocity (CAV), are used in Istanbul EEW system (Erdik et al., 2003) as a rapid detector for strong ground shaking, which is computed from the integral of the acceleration a(t) as $CAV = \int_{t_i}^{t_{max}} |a(t)| dt$. The integral of the squared velocity (IV2), defined as $IV2 = \int_{t_i}^{t} v(t)^2 dt$, is related to the early-radiated energy (Festa et al., 2008). Wang and Zhao proposed to use the squared displacement integral (ID2), specified as $IV2 = \int_{t_i}^{t_i+\tau_o} u^2 dt$, to reflect the information of different periods from advancing rupture on fault plane (Wang and Zhao, 2018). However, there are several unresolved issues, for example, the

FIGURE 3 | (A–D) show P_v, P_d, IV2, and si calculated from the first 1 s (dark circles), 2 s (blue squares), and 3 s (red triangles) of P wave data, respectively. The PGV regression relationships determined by this study are shown as solid lines, and the standard deviations are shown as dashed lines.
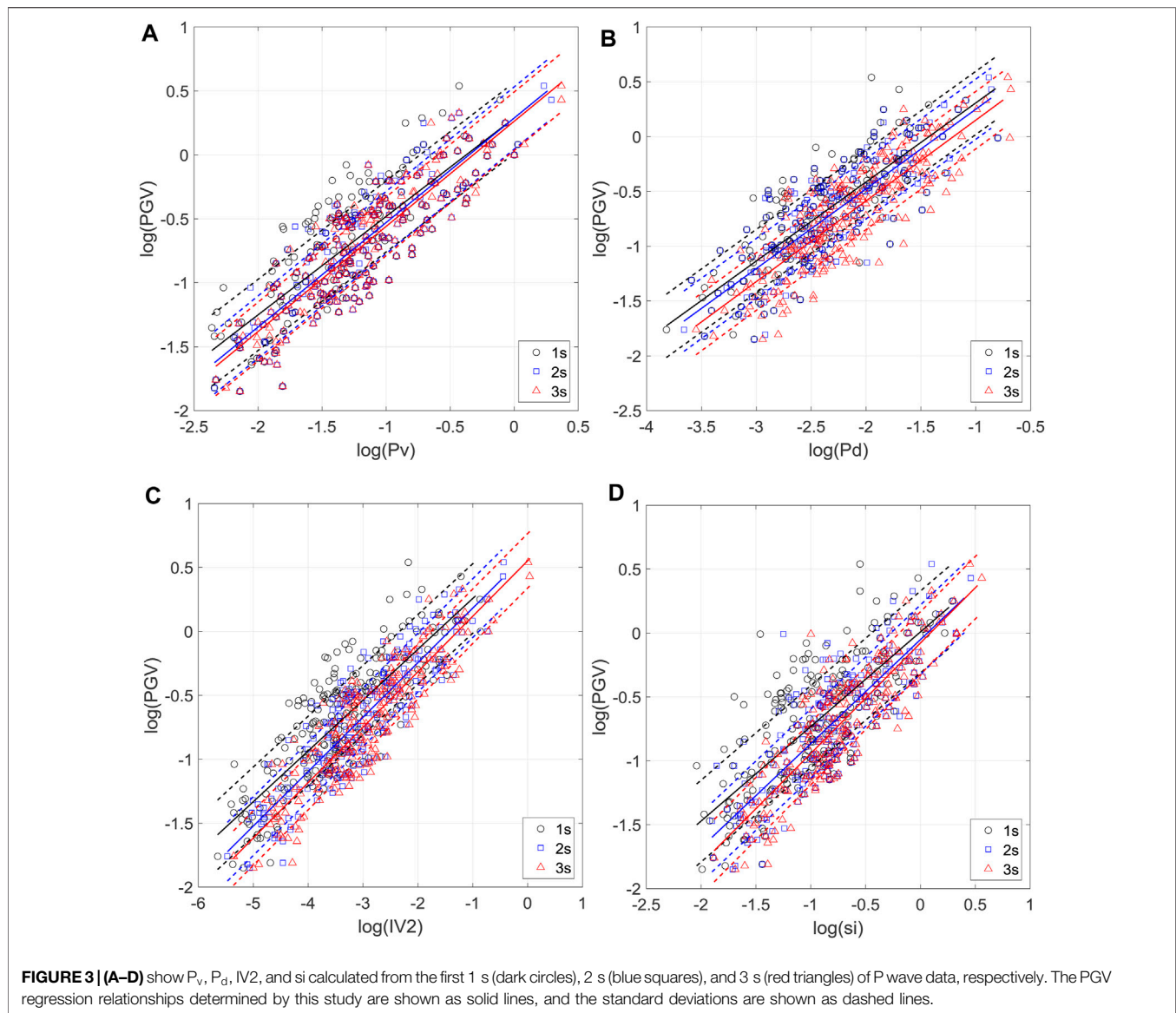
estimation accuracy and reliability, in the empirical relationships toward different ground motion parameters and to what an extent that the length of the signal window could affect the estimates.

Therefore, on the basis of the initial P wave arrival time t_i, the early-measurable parameters were investigated and a linear regression model between the ground motion and the characteristic parameters is assumed as follows:

$$\log(P_{GM}) = A \times \log(P_{EEW}) + B \pm stv \tag{2}$$

where the P_{GM} stands for the ground motion parameters, i.e., PGA, PGV, PGD, and SI, P_{EEW} stands for the EEW characteristic parameters, i.e., P_a, P_v, P_d, IA2, IV2, ID2, CAV, and si, A and B are constants that are to be determined from the regression analysis, and stv is the standard deviation.

RESULTS

Since better estimates might be obtained by expanding the observation time window to update the characteristic parameters, the time windows of 1 s to 3 s are investigated, respectively. Under the current analytical form, the resulting best-fitting regression coefficients for the four ground motion parameters and the corresponding characteristic parameters are listed in **Tables 2**, **5**.

With the calculated standard deviation stv and the coefficient of determination R^2, the leading characteristic parameters for better estimating the ground motion parameters are selected. As for PGA, among the investigated parameters, P_a, IA2, and CAV could be good estimators that the corresponding stv reduce to 0.195, 0.184, and 0.186 while the R^2 rise to 0.823, 0.843, and 0.841 of a 3-s window, respectively. With regard to PGV, the

FIGURE 4 | (A–B) show P_d and ID2 calculated from the first 1 s (dark circles), 2 s (blue squares), and 3 s (red triangles) of P wave data, respectively. The PGD regression relationships determined by this study are shown as solid lines, and the standard deviations are shown as dashed lines.
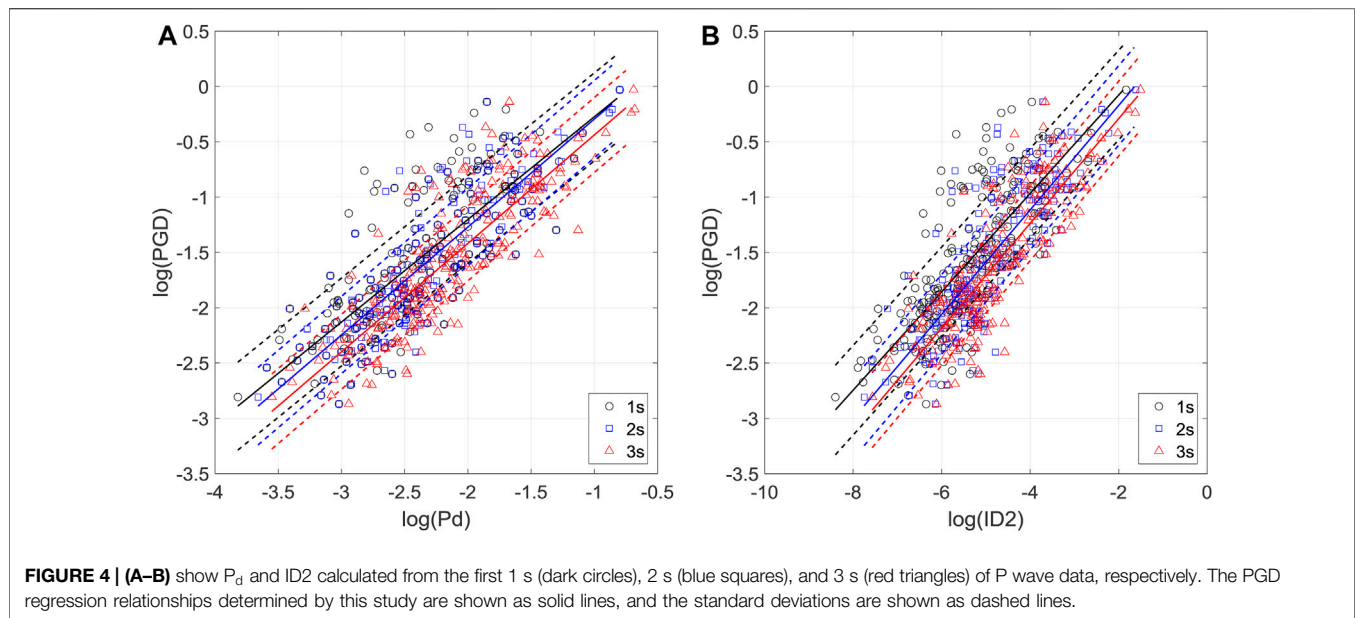
characteristic parameters P_v, P_d, IV2, and si could give a better estimation that the stv are equal to 0.229, 0.262, 0.213, and 0.248 while the R^2 equal 0.772, 0.702, 0.803, and 0.742 of a 3-s window, respectively. In addition, the characteristic parameters correlate with displacement, i.e., P_d and ID2 are suitable for estimating PGD that the stv of the two correlations are 0.338 and 0.339 while both give a R^2 of 0.715 considering a 3-s window, respectively. In regard to SI, the characteristic parameters P_v, P_d, and IV2 could get good results that the stv are 0.247, 0.253, and 0.226 while the R^2 reach to 0.741, 0.727, and 0.782 of a 3-s window. Generally, the selected characteristic parameters used for estimating PGA demonstrate a highest correlation within the analyzed data, and the situations of PGV and SI are relatively on the same level, better than that of PGD.

With the corresponding leading parameters for estimating the four ground motion parameters, **Figures 2**, **5** illustrate the linear regressions curves aiming PGA, PGV, PGD, and SI, respectively. In each figure, the characteristic parameters calculated from the first 1 s, 2 s, and 3 s are shown with circles, squares, and triangles, respectively, where the solid line refers to the regression relationship while the dashed lines stand for the standard deviations. The regression curves show that the investigated characteristic parameters correlate well with the ground motion parameters, and the uncertainties of the ground motion determination for the events reduce along with the increases of the time windows, since most of the seismic accumulated energy could be released in a short time.
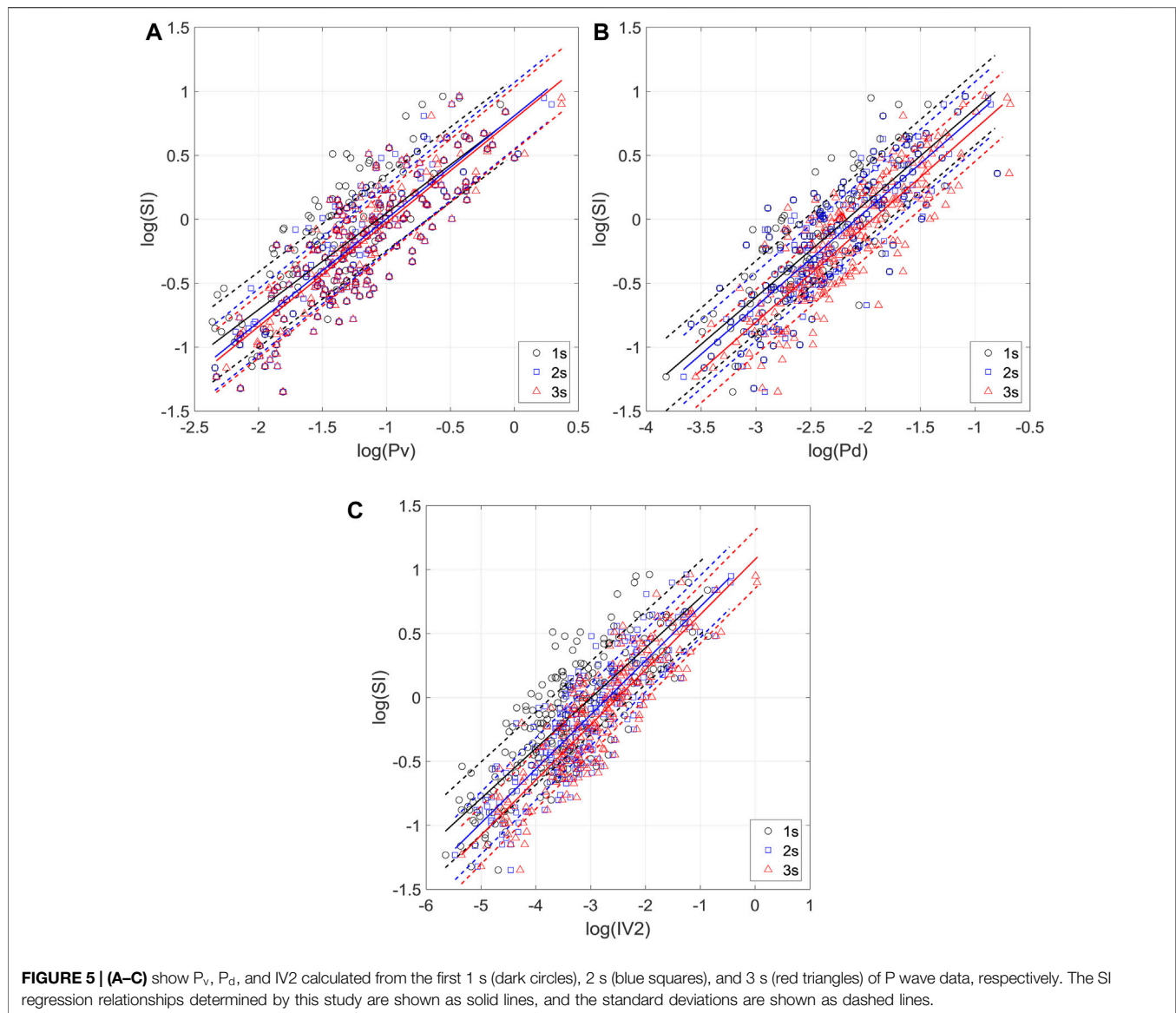
To further investigate that to what an extent the length of the initial signal window could affect the estimations, we compared the variation tendency of standard deviation and determination coefficient between the leading parameters and the corresponding ground motion parameters of different time window, which are shown in **Figure 6**. From the variation slope of each investigated parameter, both stv and R^2 could reflect the correlations with the increasing of the time window. For most cases, there is a

significant stv reduction and R^2 increase while a gentle change for 1–2 s and 2–3 s, respectively. Specifically, we calculated the increase rates Δ of the standard deviation stv between each time window interval for each investigated correlations, which are listed in **Table 6**, **9**. For PGA, the reduction rates of stv among the three characteristic parameters are all above 15% over 1 to 2 s, where the IA2 has the highest rate of 18.37%, while those of the 2–3 s are reduced to 4.88–8.37%. With regard to PGV, the performance of P_v, IV2, and si demonstrated a similar trend as parameters for PGA, while which of P_d is slight small, giving a decrease rate of 4.84% for 1–2 s and 4.73% for 2–3 s, respectively. As for PGD and SI, except for P_d who performed similar as the case for PGV, the decrease rates of stv of other characteristic parameters are around 11.11–14.74% over 1–2 s and 3.43–7.0% over 2–3 s.

DISCUSSION AND CONCLUSION

In this paper, the proposed method is envisaged to be based on a single station and is expected to improve the reliability of an on-site system, where no information or constraint on the earthquake source is available in real-time. Aiming at the ground motion estimation using the initial P wave, we have investigated the continuous measurement of eight attributes for the fast prediction of the expected shaking at the same site, where the estimation accuracy and reliability toward different ground motion parameters and to what an extent that the length of the signal window could affect the estimates are proposed. Although the single station method is conceived, the methodology proposed here could be easily integrated in a network-based EEW platform.

The EEW characteristic parameters, i.e., P_a, P_v, P_d, IA2, IV2, ID2, CAV, and si values, for the selected aftershocks (4.0 ≤ Ms ≤ 6.5) of the 2008 Wenchuan earthquake were calculated,

FIGURE 5 | (A–C) show P_v, P_d, and IV2 calculated from the first 1 s (dark circles), 2 s (blue squares), and 3 s (red triangles) of P wave data, respectively. The SI regression relationships determined by this study are shown as solid lines, and the standard deviations are shown as dashed lines.
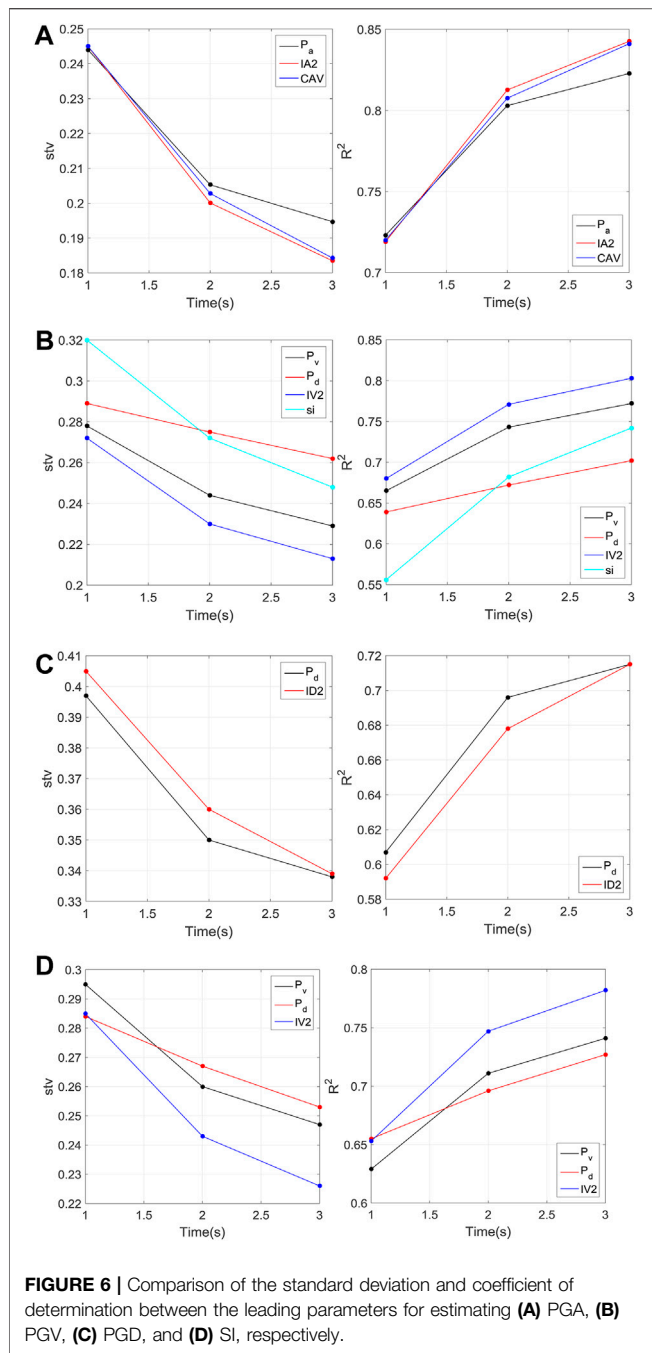
and regression relationships between each of these parameters and ground motion parameters, i.e., PGA, PGV, PGD, and SI, were established, respectively. Our results show that for PGA, the characteristic parameters P_a, IA2, and CAV could be good estimators and for PGV, the P_v, P_d, IV2, and si could give a better estimation. The P_d and ID2 are suitable for estimating PGD while in regard to SI, the P_v, P_d, and IV2 could get good results. Therefore, for different ground motion parameters, using an appropriate parameter is necessary while it also could be suggested to combine two of the possible parameters together in the real EEW operations. In addition, the predicted peak ground shaking can be used to determine the expected intensity, through a regression relationship.

The integral quantities, i.e., IV2, ID2, and CAV, are directly correlated with the radiated energy E in the initial stages of seismic ruptures, which are often used to correlate the final earthquake size (Allen et al., 2009; Colombelli and Zollo,

2016). However, in this study, it is found these parameters could also link ground motion parameters. In addition, we also found that the frequency parameter si could correlate ground motion parameters (e.g., PGA and PGV that reflect the ground shaking intensity) well. Since the observation stations were mainly set on soil conditions, it is inferred that this frequency parameter can reflect information of site effects.

Since time is the key parameter of the early warning system, the longer the available time before the disaster phenomenon reaches the target, the more effective and comprehensive the countermeasures can be taken. In contrast of regional EEW systems, which yield more accurate estimates of the source parameters, the on-site EEW systems could provide faster warning times for near-source targets at the price of a lower accuracy on the estimation of earthquake parameters. There is always a trade-off between the early warning time and the reliability of earthquake information. From our results, a 2-s

FIGURE 6 | Comparison of the standard deviation and coefficient of determination between the leading parameters for estimating **(A)** PGA, **(B)** PGV, **(C)** PGD, and **(D)** SI, respectively.

TABLE 6 | Comparison of the standard deviation stv between the leading 3 parameters for estimating PGA.

PGA	P_a		IA2		CAV	
	stv	Δ (%)	stv	Δ (%)	stv	Δ (%)
1	0.244	15.98	0.245	18.37	0.245	17.14
2	0.205	4.88	0.200	8.00	0.203	8.37
3	0.195		0.184		0.186	

TABLE 7 | Comparison of the standard deviation stv between the leading 4 parameters for estimating PGV.

PGV	P_v		P_d		IV2		si	
	stv	Δ (%)	stv	Δ (%)	stv	Δ (%)	stv	Δ (%)
1	0.278	12.23	0.289	4.84	0.272	15.44	0.320	15.00
2	0.244	6.15	0.275	4.73	0.230	7.39	0.272	8.82
3	0.229		0.262		0.213		0.248	

TABLE 8 | Comparison of the standard deviation stv between the leading 2 parameters for estimating PGD.

PGD	P_d		ID2	
	stv	Δ (%)	stv	Δ (%)
1	0.397	11.84	0.405	11.11
2	0.350	3.43	0.360	5.83
3	0.338		0.339	

TABLE 9 | Comparison of the standard deviation stv between the leading 3 parameters for estimating SI.

SI	P_v		P_d		IV2	
	stv	Δ (%)	stv	Δ (%)	stv	Δ (%)
1	0.295	11.86	0.284	5.99	0.285	14.74
2	0.260	5.00	0.267	5.24	0.243	7.00
3	0.247		0.253		0.226	

window could effectively improve the estimation accuracy by approximately 11.5–18.5% compared with using a 1-s window, as the window increases to 3 s, the accuracy would further improve while the growth rate will be reduced to around 3.0–8.0%. That is to say, for appropriate correlations between the characteristic parameters and ground motion parameters, a 2 s initial P wave might be enough for the first alert; meanwhile, the updating procedures should be considered certainly in real operations.

The 2008 Ms 8.0 Wenchuan earthquake occurred along the Longmenshan faults (Li et al., 2008), consisting of mountain-front fault, central fault, and mountain-back fault, which are situated in the transitional area from the Tibetan Plateau to the South China Plate. This complicated geological and topographic environment caused complex focal mechanisms, propagation processes, and site effects, resulting in the ground motions to have the nature of complexity. Because aftershocks distribute on different secondary faults, their focal mechanisms present complex local tectonic stress field and even vary with time. Generally, for the southern segment, the thrust component is stronger than strike-slip component, while the northern segment corresponds to a section of mostly strike-slip mechanism; the middle segment may be related to the transition between the southern and northern segments (Zheng et al., 2010; Yi et al., 2012), since the used data cover the general magnitude gradients that are of concern for EEW systems, and multiple stations recorded the wave forms for each event within the specified range, providing important benefits for EEW studies. In addition, the earthquake rupture and the propagation process should be

investigated and studied to develop a better theoretical research of the phase nature.

The paper tested different attributes for the fast prediction of the expected shaking in real-time, while practical operations require consideration of other aspects. For example, the observation stations should be built with the ability to provide early warnings that the detection instruments are capable of improving the signal quality, especially for the vertical component. In addition, appropriate investigations of the observation locations with detailed surrounding seismic environments are also necessary. When calibrating the proposed method for a specific area, the possible impact of site effect, which may produce local, systematic amplification/attenuation of the perceived shaking, is required to have a detailed analysis.

DATA AVAILABILITY STATEMENT

The original contributions presented in the study are included in the article/Supplementary Material; further inquiries can be directed to the corresponding author.

REFERENCES

Allen, R. M., and Melgar, D. (2019). Earthquake Early Warning: Advances, Scientific Challenges, and Societal Needs. *Annu. Rev. Earth Planet. Sci.* 47, 361–388. doi:10.1146/annurev-earth-053018-060457

Allen, R. M., Gasparini, P., Kamigaichi, O., and Böse, M. (2009). The Status of Earthquake Early Warning Around the World: An Introductory Overview. *Seismological Res. Lett.* 80, 682–693. doi:10.1785/gssrl.80.5.682

Boore, D. M., Stephens, C. D., and Joyner, W. B. (2002). Comments on Baseline Correction of Digital strong-motion Data: Examples from the 1999 Hector Mine, California, Earthquake. *Bull. Seismological Soc. America* 92, 1543–1560. doi:10.1785/0120000926

Bose, M., Hauksson, E., Solanki, K., Kanamori, H., Wu, Y.-M., and Heaton, T. H. (2009). A New Trigger Criterion for Improved Real-Time Performance of Onsite Earthquake Early Warning in Southern California. *Bull. Seismological Soc. America* 99 (2A), 897–905. doi:10.1785/0120080034

China Strong Motion Networks Centre (2020). China Strong Motion Networks Centre. Available at: www.cenc.ac.cn (Accessed November 05, 2020).

Colombelli, S., Caruso, A., Zollo, A., Festa, G., and Kanamori, H. (2015). A P Wave-based, On-site Method for Earthquake Early Warning. *Geophys. Res. Lett.* 42, 1390–1398. doi:10.1002/2014gl063002

Colombelli, S., and Zollo, A. (2016). Rapid and Reliable Seismic Source Characterization in Earthquake Early Warning Systems: Current Methodologies, Results, and New Perspectives. *J. Seismol.* 20 (4), 1–16. doi:10.1007/s10950-016-9570-z

Cremen, G., and Galasso, C. (2020). Earthquake Early Warning: Recent Advances and Perspectives. *Earth-Science Rev.* 205, 103184. doi:10.1016/j.earscirev.2020.103184

Erdik, M., Fahjan, Y., Ozel, O., Alcik, H., Mert, A., and Gul, M. (2003). Istanbul Earthquake Rapid Response and the Early Warning System. *Bull. Earthquake. Eng.* 1, 157–163. doi:10.1023/a:1024813612271

Festa, G., Zollo, A., and Lancieri, M. (2008). Earthquake Magnitude Estimation from Early Radiated Energy. *Geophys. Res. Lett.* 35, L22307. doi:10.1029/2008gl035576

Hoshiba, M. (2014). Review of the Nationwide Earthquake Early Warning in Japan during its First Five Years. *Earthquake Hazard. Risk Disasters* 2014, 509–529. doi:10.1016/b978-0-12-394848-9.00019-5

Housner, G. W. (1952). *Intensity of Ground Motion during Strong Earthquakes.* California: California Institute of Technology.

AUTHOR CONTRIBUTIONS

ZW: conceptualization, methodology, data analysis, visualization, and writing the original draft. BZ: methodology, writing—review and editing, and supervision.

FUNDING

ACKNOWLEDGMENTS

Kanamori, H. (2005). Real-Time Seismology and Earthquake Damage Mitigation. *Annu. Rev. Earth Planet. Sci.* 33, 195–214. doi:10.1146/annurev.earth.33.092203.122626

Küperkoch, L., Meier, T., Lee, J., and Friederich, W.EGELADOS Working Group (2010). Automated Determination of P-phase Arrival Times at Regional and Local Distances Using Higher Order Statistics. *Geophys. J. Int.* 181, 1159–1170. doi:10.1111/j.1365-246x.2010.04570.x

Li, Z. Q., Yuan, Y. F., Li, X. L., and Zeng, J. (2008). Preliminary Research on the Characteristics of the Ms 8.0 Wenchuan Earthquake hazard. *Seismol. Geol.* 30 (4), 855–876.

Nakamura, Y., Saita, J., and Sato, T. (2011). On an Earthquake Early Warning System (EEW) and its Applications. *Soil Dyn. Earthquake Eng.* 31, 127–136. doi:10.1016/j.soildyn.2010.04.012

Satriano, C., Wu, Y.-M., Zollo, A., and Kanamori, H. (2011). Earthquake Early Warning: Concepts, Methods and Physical Grounds. *Soil Dyn. Earthquake Eng.* 31, 106–118. doi:10.1016/j.soildyn.2010.07.007

Wang, Z., and Zhao, B. (2017). Automatic Event Detection and Picking of P, S Seismic Phases for Earthquake Early Warning and Application for the 2008 Wenchuan Earthquake. *Soil Dyn. Earthquake Eng.* 97, 172–181. doi:10.1016/j.soildyn.2017.03.017

Wang, Z., and Zhao, B. (2018). Method of Accurate-Fast Magnitude Estimation for Earthquake Early Warning -----Trial and Application for the 2008 Wenchuan Earthquake. *Soil Dyn. Earthquake Eng.* 109, 227–234. doi:10.1016/j.soildyn.2018.03.006

Wu, Y.-M., and Kanamori, H. (2008). Development of an Earthquake Early Warning System Using Real-Time strong Motion Signals. *Sensors* 8 (1), 1–9. doi:10.3390/s8010001

Wu, Y.-M., and Kanamori, H. (2005). Rapid Assessment of Damage Potential of Earthquakes in Taiwan from the Beginning of P Waves. *Bull. Seismological Soc. America* 95 (3), 1181–1185. doi:10.1785/0120040193

Xu, X., Wen, X., Yu, G., Chen, G., Klinger, Y., Hubbard, J., et al. (2009). Coseismic Reverse- and Oblique-Slip Surface Faulting Generated by the 2008 Mw 7.9 Wenchuan Earthquake, China. *Geology* 37, 515–518. doi:10.1130/g25462a.1

Yi, G. X., Long, F., and Zhang, Z. W. (2012). Spatial and Temporal Variation of Focal Mechanisms for Aftershocks of the 2008 Ms8.0 Wenchuan Earthquake. *Chin. J. Geophys.* 55 (4), 1213–1227.

Zheng, Y., Ni, S., Xie, Z., Lv, J., Ma, H., and Sommerville, P. (2010). Strong Aftershocks in the Northern Segment of the Wenchuan Earthquake Rupture Zone and Their Seismotectonic Implications. *Earth Planet. Sp* 62 (11), 881–886. doi:10.5047/eps.2009.06.001

Zollo, A., Amoroso, O., Lancieri, M., Wu, Y.-M., and Kanamori, H. (2010). A Threshold-Based Earthquake Early Warning Using Dense Accelerometer Networks. *Geophys. J. Int.* 183, 963–974. doi:10.1111/j.1365-246x.2010.04765.x

Zollo, A., Colombelli, S., and Emolo, A. (2016). An Integrated Regional and On-Site Earthquake Early Warning System for Southern Italy: Concepts, Methodologies and Performances. *Early Warning Geol. Disasters, chapter 7,* 117–137. doi:10.1007/978-3-642-12233-0_7